Supporting Information for

What is Special about Silicon in Functionalised Organic Semiconductors?

Karl J. Thorley,[†‡]* Micai Benford,[§] Yang Song,[§] Sean R. Parkin,[†] Chad Risko[†‡] and John E. Anthony.[†‡]

†University of Kentucky, Department of Chemistry, Lexington KY 40508, USA

‡University of Kentucky, Center for Applied Energy Research, Lexington KY 40511, USA

§Centre College, Department of Chemistry, Danville KY 40422, USA

Contents

General Experimental Information

Anhydrous tetrahydrofuran, lithium diisopropylamide, n-butyllithium, methyllithium, and diethylchlorophosphate were purchased from Sigma Aldrich. Acetonitrile and diethyl ether were purchased from VWR. Bromoethane was purchased from Oakwood. All purchased chemicals were used without further purification. FADT quinone,[1] TES-FADT,[1] and TEG-FADT[2] were synthesised as reported.

Proton and carbon NMR spectra were collected using a 400 MHz JEOL spectrometer. Chemical shifts of each spectrum are reported in ppm and referenced to deuterated chloroform solvent. HRMS was measured using a ThermoFisher Q-Exactive spectrometer by ESI in positive mode using a 10 µg/mL solution in 1:1 acetonitrile/water. GC-MS analysis was performed using a Scion-SQ spectrometer with a Bruker BR-5HT column (15 m, 0.25 mm ID, 0.10 µm df). Method details are provided with the copies of chromatograms. UV-visible spectra were measured using a Cary 60 UV-Vis spectrometer using a 10 mm cuvette and solutions approximately 10^{-6} M. Fluorescence spectra were collected using a StellarNet Inc SilverNova spectrophotometer with an SL1-LED excitation source using a 10 mm cuvette and solutions approximately 10^{-6} M. Cyclic voltammetry was measured using a BAS CV-50W potentiostat at a scan rate of 50 mV/s with a button glassy carbon working electrode, a platinum wire counter electrode and an Ag/AgCl reference electrode. A solution of 0.1 M Bu_4NPF_6 in dichloromethane was used as a supporting electrolyte solution under a blanket of N_2 with Fc/Fc^+ as an internal reference. Infrared spectra were collected using a Perkin Elmer Frontier(TM) FT-IR Spectrometer equipped with a RFSH 1 Bounce Diamond/zinc selenide (ZnSe) top plate assay.

Synthetic Procedures

2,2-Diethylbutanenitrile 1[3]: Acetonitrile (2.0 mL, 38.2 mmol) and bromoethane (9.91 mL, 133.7 mmol) were dissolved in dry THF (120 mL) in a round bottom flask, and cooled to 0 °C. Lithium diisopropylamide (1M, 126.0 mL, 126.0 mmol) was added slowly. The reaction was stirred for 1 hour at room temperature, and then quenched with H_2O (100 mL). The product was extracted with Et_2O (100 mL) and the solvent removed in vacuo. The crude product was passed through a short silica plug with CH_2Cl_2 and distilled under reduced pressure by Kugelrohr to yield the clean product as a clear oil (4.59 g, 96 %)

^{1}H NMR (400 MHz, CDCl$_3$) δ 1.51 (q, J = 7.5 Hz, 2H), 0.91 (t, J = 7.5 Hz, 3H); ^{13}C NMR (101 MHz, CDCl$_3$) δ 123.8, 42.1, 27.9, 8.5

HRMS m/z (ESI) $C_8HN + H^+$ requires 126.1277, observed 126.1278

3,3-Diethylpentan-2-one 2[4]: Nitrile **1** (2.5 g, 19.96 mmol) was dissolved in Et_2O (100 mL) and cooled to 0 °C. Methyllithium solution (1.6 M in Et_2O, 18.7 mL, 29.95 mmol) was added slowly, and the mixture stirred for 5 hours at room temperature. The reaction was quenched with H_2O (100 mL), the organic layer was separated and the aqueous layer washed with Et_2O (100 mL). The crude material was redissolved in THF (100 mL) and saturated NH_4Cl (aq) solution (100 mL) was added. The reaction was stirred overnight at room temperature. The product was then extracted with Et_2O and the solvent removed. The mixture was passed through a silica plug with CH_2Cl_2 to yield the crude product, and then with EtOAc to recover intermediate imine whose hydrolysis could be repeated by stirring with saturated NH_4Cl. Combined fractions of ketone product were combined and distilled at reduced pressure by Kugelrohr to yield clean product as a clear oil (1.16 g, 41 %).

^{1}H-NMR (400 MHz, CDCl$_3$) δ 2.06 (s, 3H), 1.54 (q, J = 7.5 Hz, 6H), 0.69 (t, J = 7.5 Hz, 9H)

^{13}C-NMR (101 MHz, CDCl$_3$) δ 214.4, 55.1, 25.6, 25.3, 8.2

HRMS m/z (ESI) $C_9H_{18}O + H^+$ requires 143.1430, observed 143.1431

3,3-Diethylpentyne 3[5]: Methyl ketone **2** (1.0 g, 7.0 mmol) was dissolved in dry THF (15 mL) and cooled to -78 °C. Lithium diisopropylamide solution (1M, 7.7 mL, 7.7 mmol) was added and the reaction stirred at -78 °C for 1 hour. Diethyl chlorophosphate (1.14 mL, 7.87 mmol) was then added, and the reaction was allowed to warm to room temperature and stirred for 5 hours. The mixture was cooled to -78 °C, and lithium diisopropylamide solution (1M, 14.06 mL, 14.06 mmol). The mixture was allowed to slowly warm to room temperature and then stirred for 16 hours. The reaction was then quenched with H_2O (50 mL) and extracted with Et_2O (50 mL). Solvent was very carefully removed under reduced pressure due to the low boiling point of the product. The crude mixture was passed through a silica plug with hexanes to yield the alkyne product as a clear oil (0.65 g, 75 %).

^{1}H-NMR (400 MHz, CDCl$_3$) δ 2.07 (s, 1H), 1.44 (q, J = 7.5 Hz, 6H), 0.90 (t, J = 7.4 Hz, 9H)

^{13}C-NMR (101 MHz, CDCl$_3$) δ 90.4, 69.4, 39.3, 29.7, 8.6

m/z (ESI) could not be ionized

TEC-FADT: Alkyne **3** (0.87 g, 7.0 mmol) was dissolved in hexanes (60 mL) and cooled to 0 °C. n-Butyllithium (2.5M, 2.25 mL, 5.6 mmol) was added slowly, and the mixture stirred for 1 hour. FADT quinone[1] (0.500 g, 1.4 mmol) was added in one portion and the mixture stirred at room temperature for 16 hours. The reaction was quenched by addition of saturated NH_4Cl solution (5 mL) and the mixture poured directly onto a silica plug. Excess alkyne was eluted with hexanes, and then the intermediate FADT diol was eluted with 1:1 CH_2Cl_2/acetone. After removal of the solvents, the diol was redissolved in 1:1 acetone/MeOH (100 mL). Tin(II) chloride (1.6 g, 7.0 mmol) and 10 % HCl (aq) solution (10 mL) was added, and the mixture stirred for 1 hour. The product was extracted using CH_2Cl_2 (100 mL) and then purified on silica eluting with 10:1 hexanes/CH_2Cl_2. The product was recrystallised from acetone to yield orange crystals (0.320 g, 40 %).

^{1}H-NMR (400 MHz, CDCl$_3$) δ 8.86 (s, 2H), 8.80 (s, 2H), 6.78 (d, J = 2.5 Hz, 2H), 1.80 (q, J = 7.5 Hz, 12H), 1.16 (tt, J = 7.4, 2.1 Hz, 18H) ^{13}C NMR (101 MHz, CDCl$_3$) δ 167.0, 164.1, 161.6, 140.6, 139.3, 136.1, 133.3, 129.9, 120.9, 120.4, 110.2, 102.7, 41.3, 30.2, 9.2

m/z (ESI) $C_{36}H_{36}F_2S_2^{+\bullet}$ requires 570.2221, observed 570.2196

Copies of NMR spectra
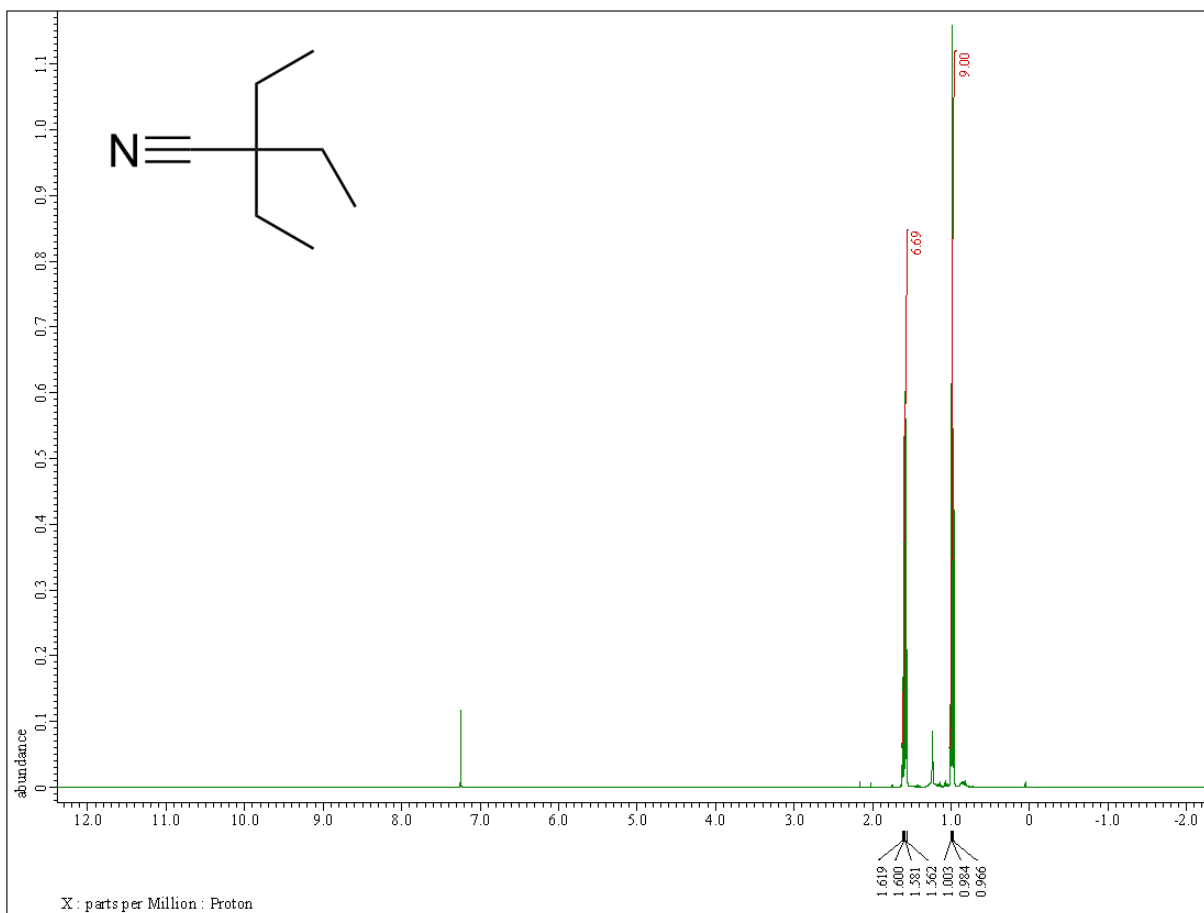
Figure S 1. ^{1}H NMR of 2,2-diethylbutanenitrile **1** measured in CDCl$_3$ at 298 K.
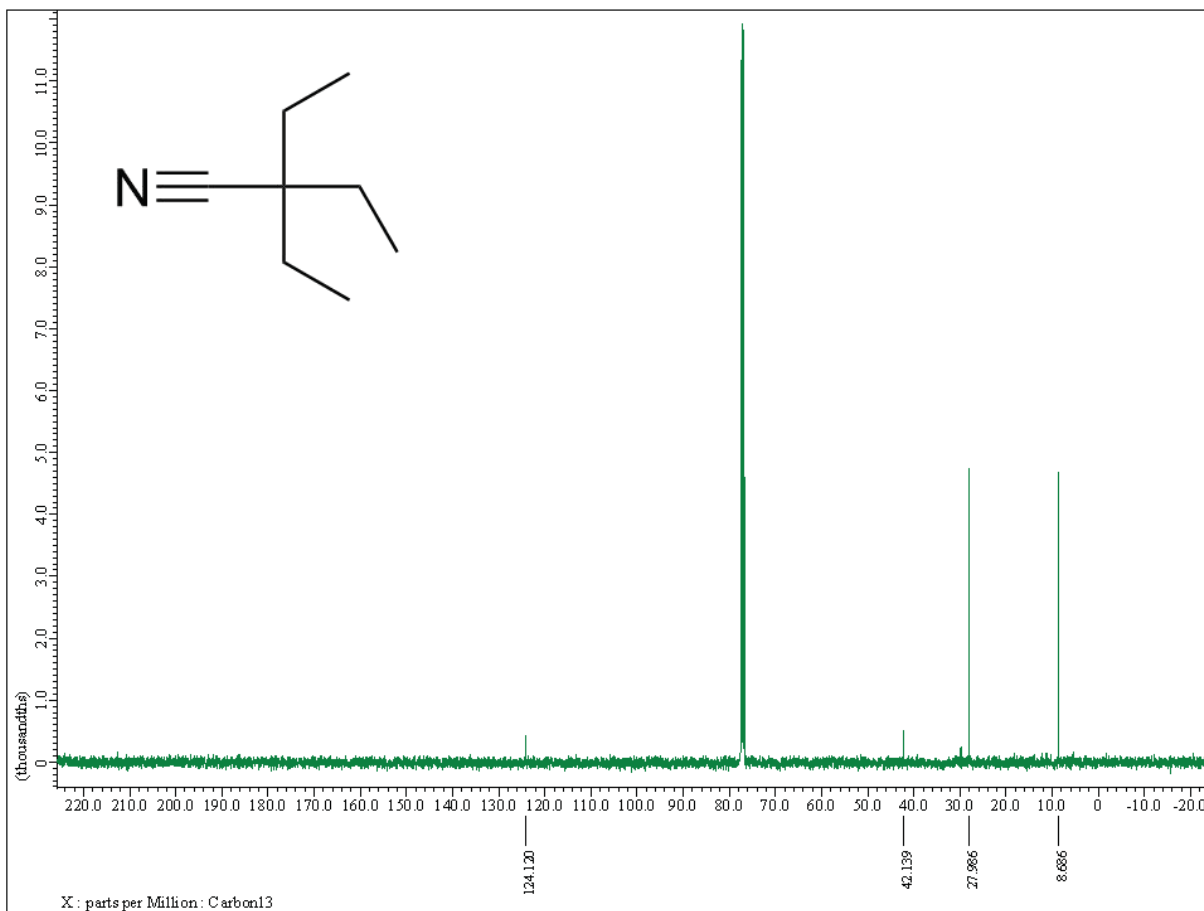
Figure S 2. ^{13}C NMR of 2,2-diethylbutanenitrile **1** measured in CDCl$_3$ at 298 K.
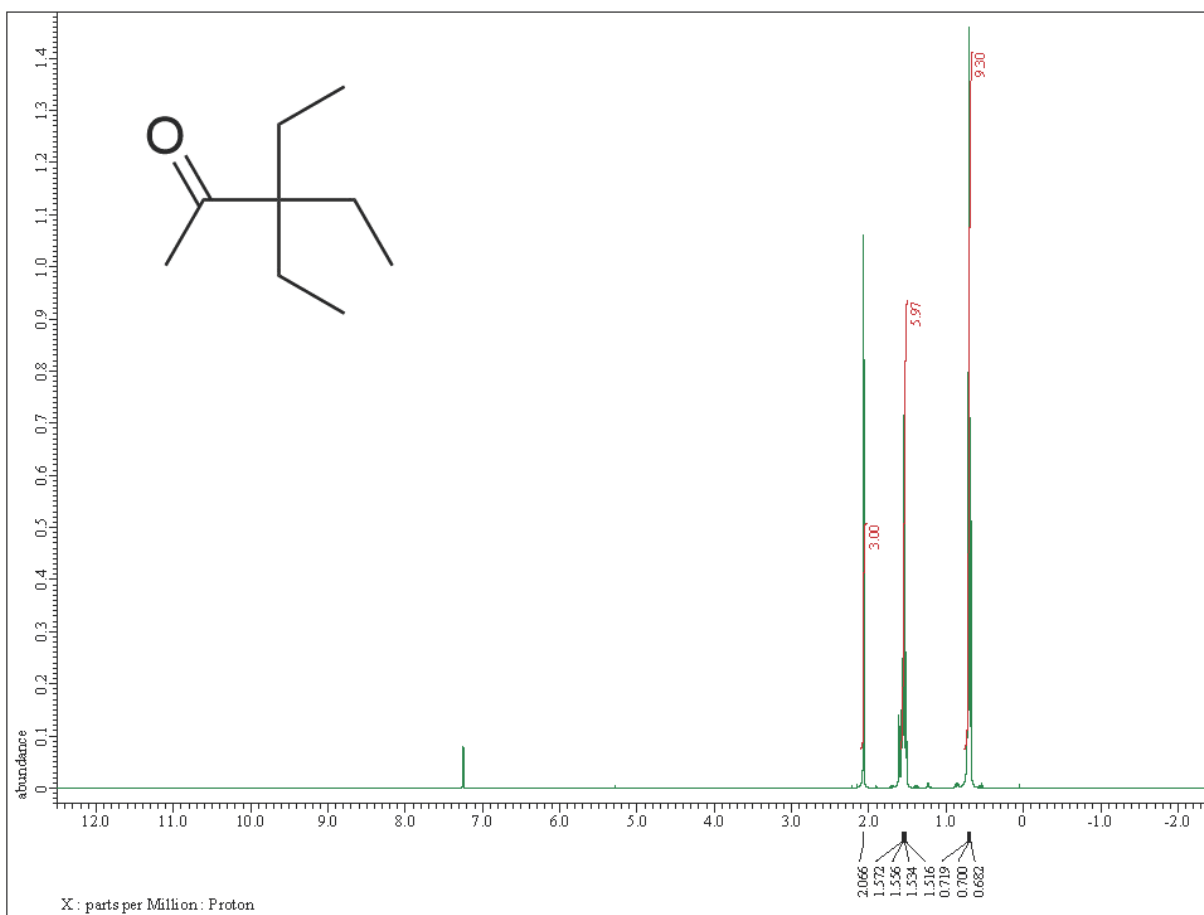
Figure S 3. ^{1}H NMR of 3,3-diethylpentan-2-one **2** measured in CDCl$_3$ at 298 K.
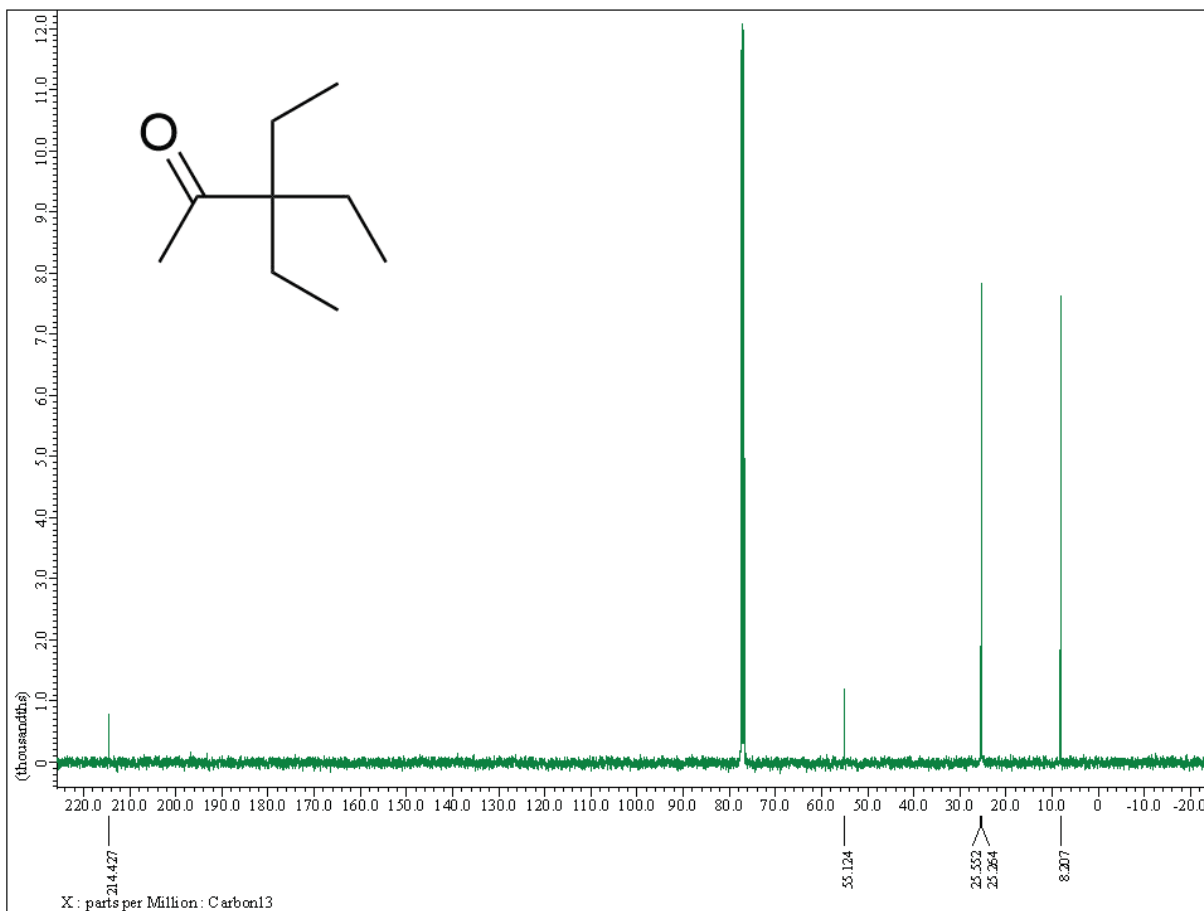
Figure S 4. ^{13}C NMR of TEC-FADT measured in CDCl$_3$ at 298 K.
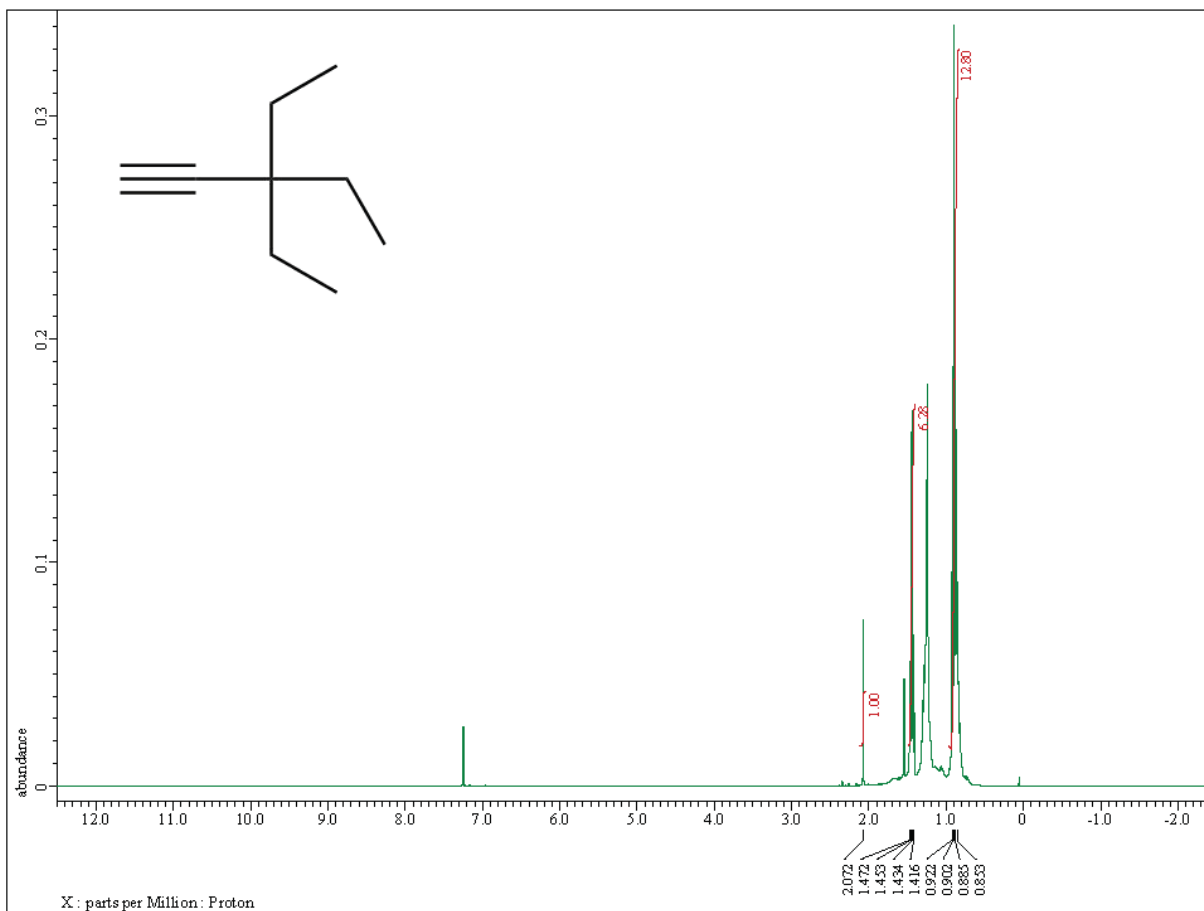
Figure S 5. ^{1}H NMR of 3,3-diethylpentyne **3** measured in CDCl$_3$ at 298 K. The sample also contains some hexanes (mixture of isomers).
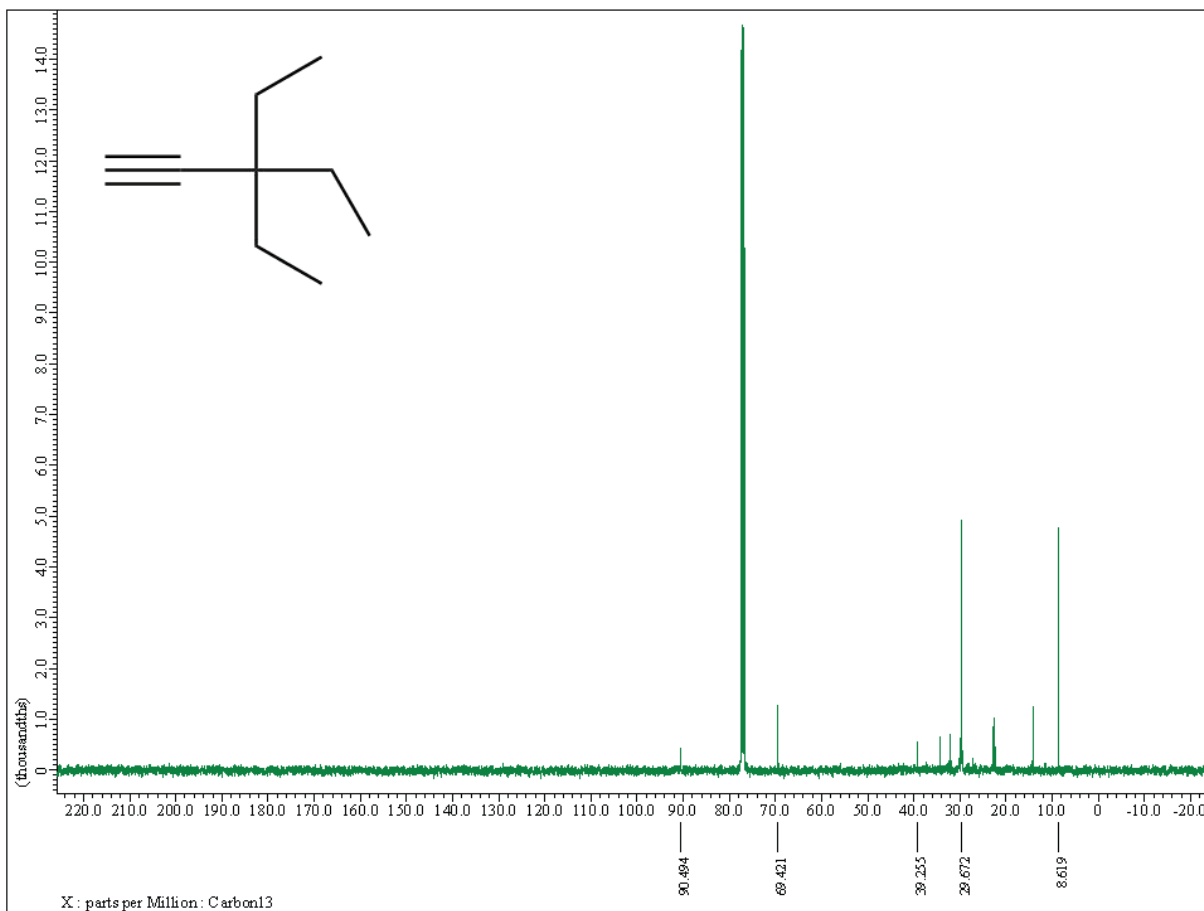
Figure S 6. ^{13}C NMR of 3,3-diethylpentyne **3** measured in CDCl$_3$ at 298 K. The sample also contains hexanes (mixture of isomers).
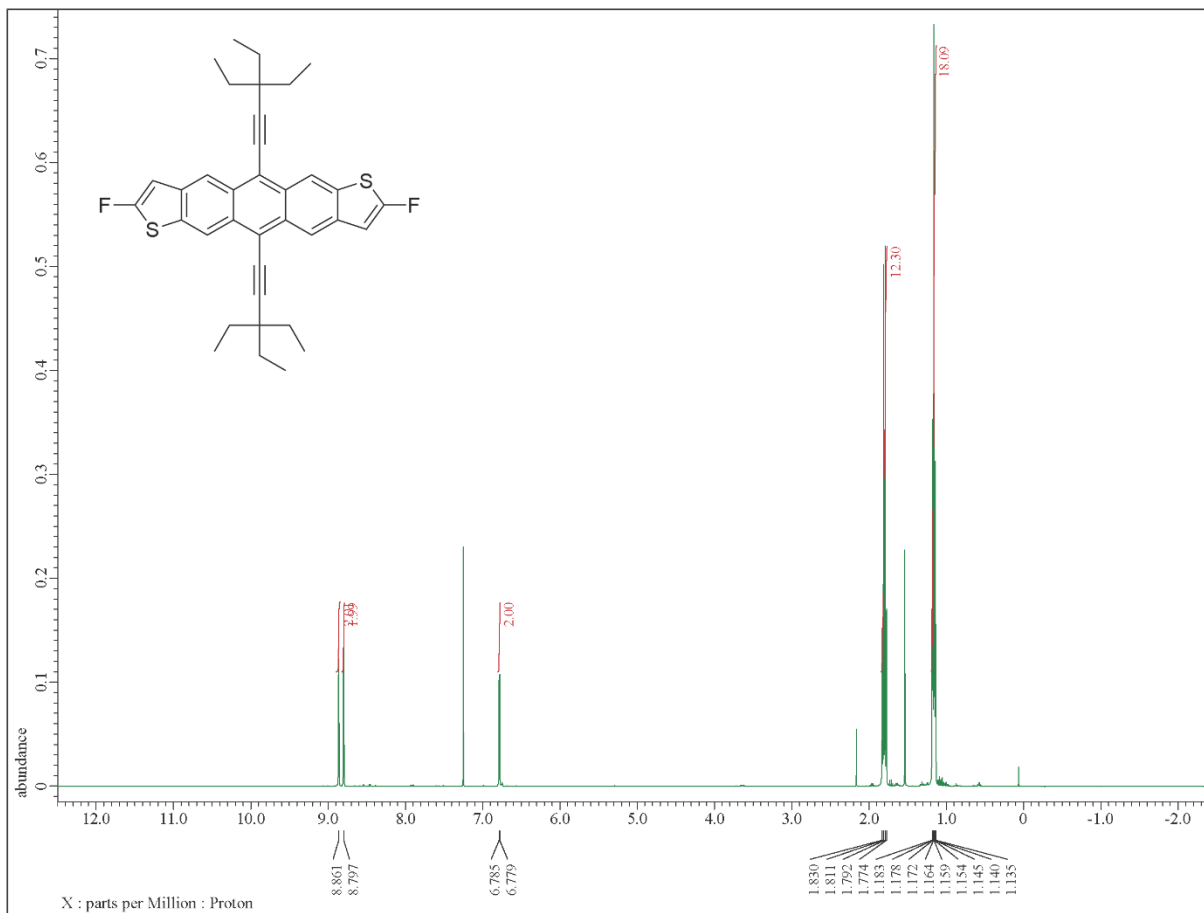
Figure S 7 ^{1}H NMR of TEC-FADT measured in CDCl$_3$ at 298 K.
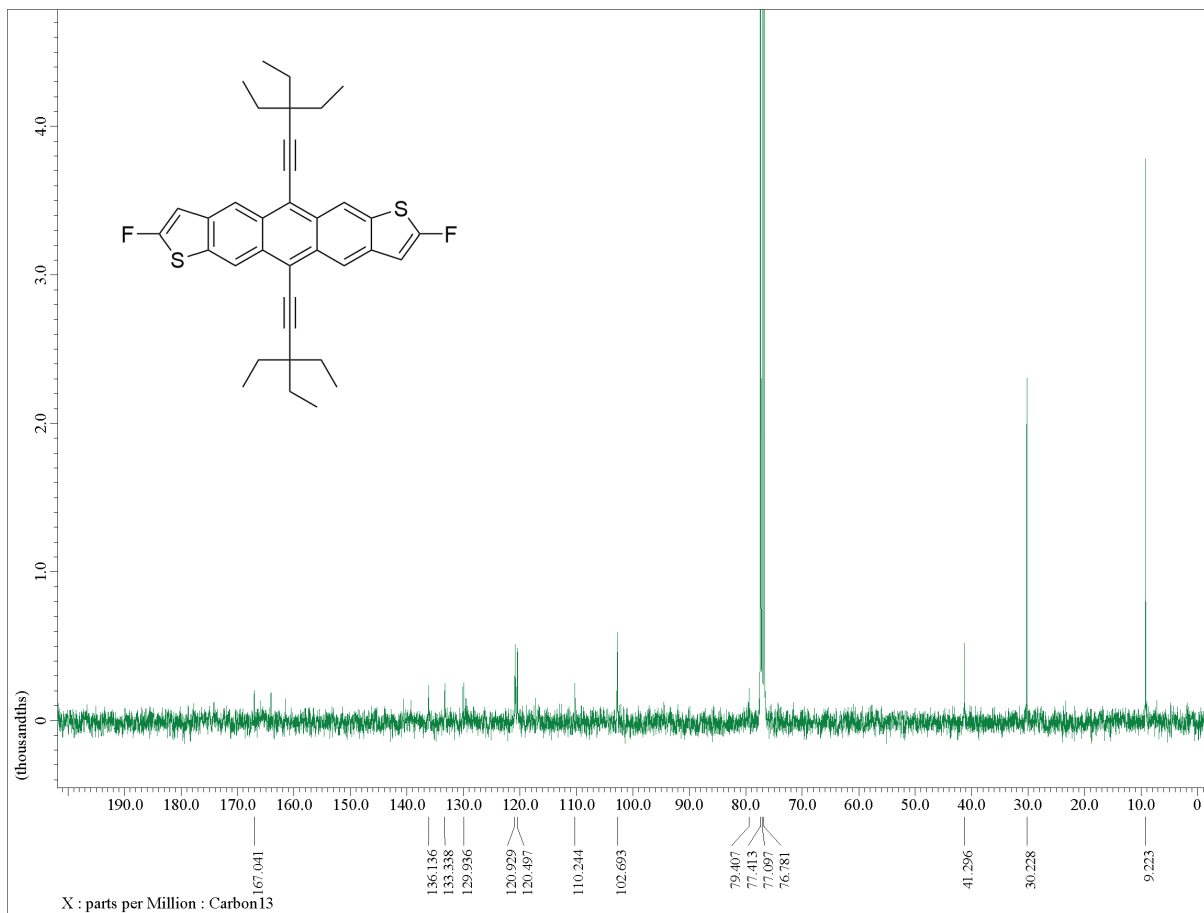
Figure S 8 ^{13}C NMR of TEC-FADT measured in CDCl$_3$ at 298 K.

GCMS data

Table S 1 Method details for GCMS analysis. Carrier gas flow rate of 1.0 mL/min.

T (°C)	Rate (°C/min)	Hold (min)	Total (min)
45.0		3.00	3.00
275.0	20.0	10.0	24.50
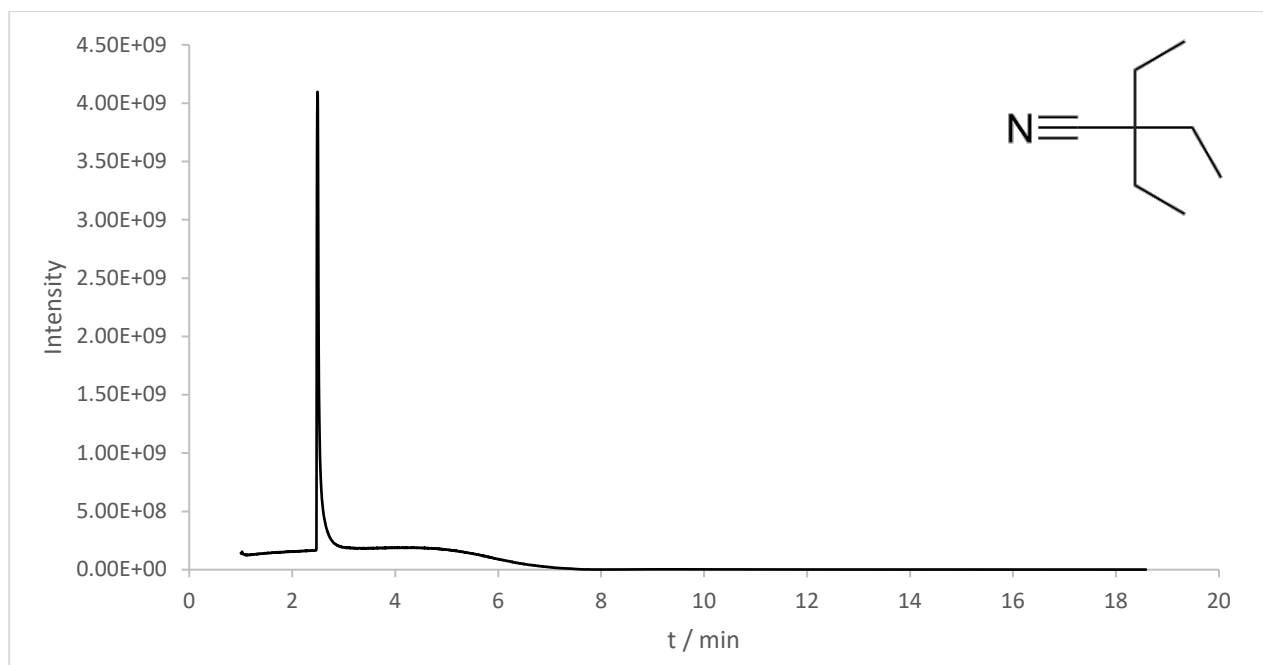
Figure S 9. Chromatogram trace for GCMS analysis of 2,2-diethylbutanenitrile **1**

Table S 2. Mass list normalised by intensity for GCMS analysis of 2,2-diethylbutanenitrile **1**

m	normalised intensity at 2.5 mins
52.08645	0.02
53.09664	0.05
54.0796	0.04
55.10486	0.34
56.12667	0.09
57.13011	0.03
66.06753	0.01
67.07475	0.09
68.09089	0.23
69.1378	0.09
70.14321	0.04
79.07524	0.01
80.08431	0.04
82.09027	1
83.1563	0.06
94.08191	0.01
95.09192	0.04
96.08853	0.07
97.09297	0.23
98.1652	0.02
110.0925	0.37
111.1508	0.03
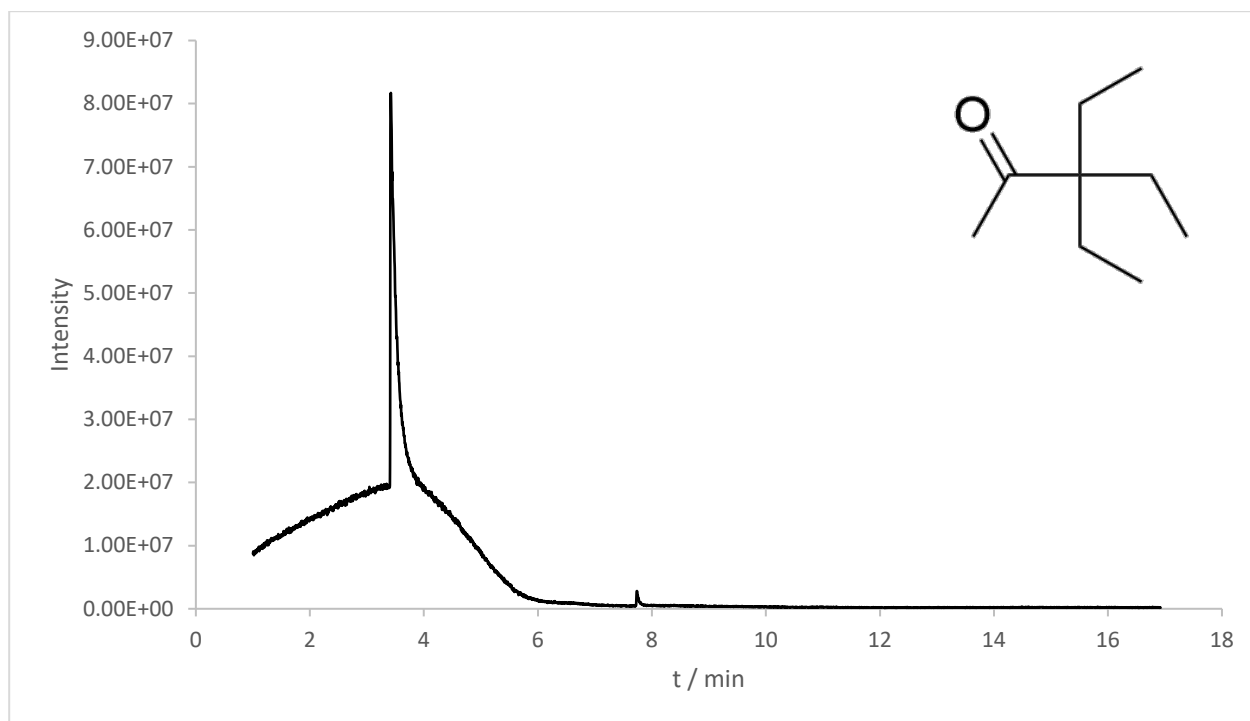
Figure S 10. Chromatogram trace for GCMS analysis of 3,3-Diethylpentan-2-one **2**. The peak around 8 minutes is from BHT stabiliser in THF.

Table S 3. Mass list normalised by intensity for GCMS analysis of 3,3-Diethylpentan-2-one **2.**

mass	normalised intensity at 3.4 mins
50.33975	0.03
51.1701	0.05
52.11024	0.01
53.19691	0.10
54.21805	0.05
55.22074	0.31
56.07379	0.08
57.18229	1.00
58.26007	0.05
65.17214	0.03
67.07103	0.12
68.1173	0.02
69.16094	0.25
70.2098	0.08
71.30256	0.02
77.11905	0.03
79.0957	0.04
81.18221	0.04
83.16659	0.07
84.15295	0.02
85.14655	0.05

91.13064	0.01
93.13069	0.01
95.27024	0.02
96.17767	0.02
97.08029	0.11
98.14518	0.27
99.13495	0.08
111.2206	0.02
112.2388	0.03
113.1969	0.02
114.1208	0.16
115.1635	0.01
125.0894	0.01
127.199	0.01
232.98	0.01
251.9703	0.02
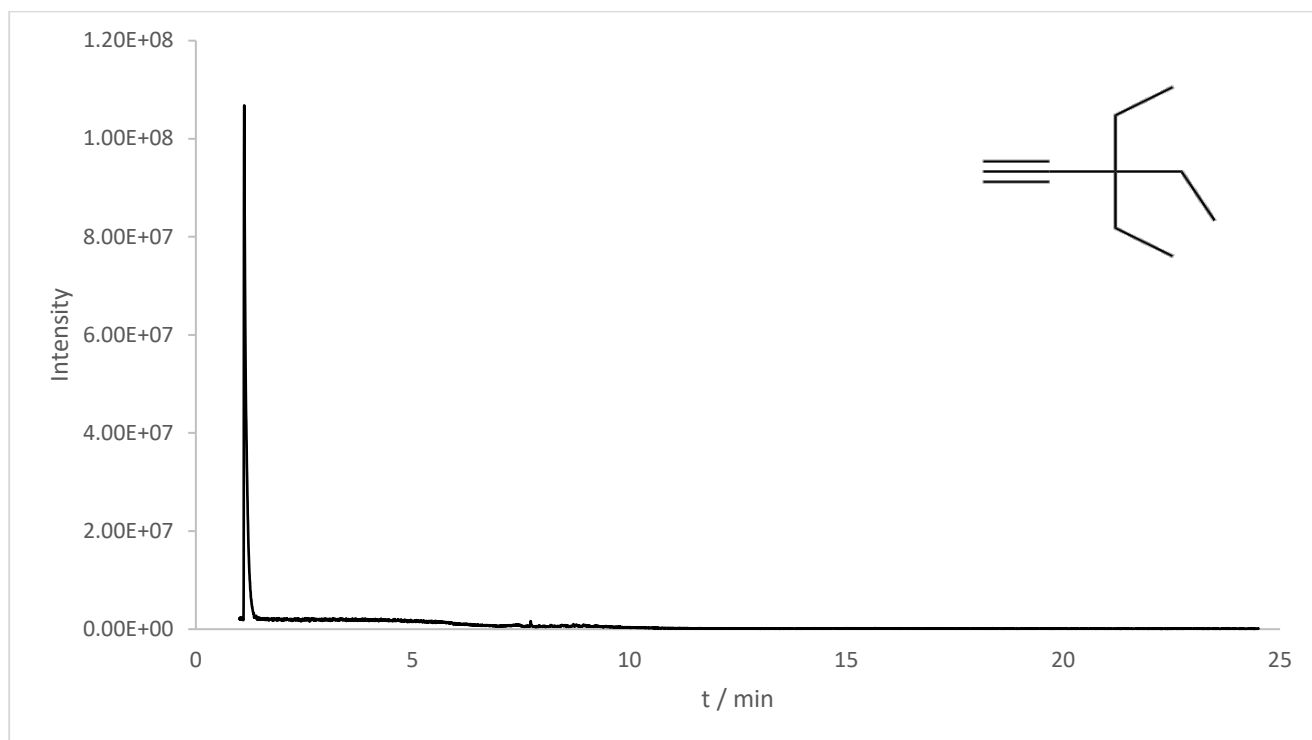
Figure S 11 Chromatogram trace for GCMS analysis of 3,3-Diethylpentyne **3**

Table S 4. Mass list normalised by intensity for GCMS analysis of 3,3-Diethylpentyne **3**

mass	normalised intensity at 1.1 mins
50.33021	0.02
51.20179	0.04
52.20383	0.02

53.22842	0.09
54.20796	0.02
55.22293	0.28
56.13065	0.08
57.19757	1
58.32819	0.04
65.14852	0.03
66.1437	0.01
67.15106	0.1
68.156	0.03
69.19132	0.24
70.27618	0.06
71.30515	0.01
77.07375	0.03
79.15833	0.04
81.15207	0.04
82.99641	0.05
84.12928	0.02
85.14939	0.05
95.11837	0.02
96.07006	0.02
97.12048	0.09
98.16523	0.25
99.15404	0.08
111.3986	0.02
112.2264	0.03
113.1156	0.02
114.1309	0.16
115.2008	0.01
125.2061	0.01
249.9987	0.01

X-ray Crystallography

X-ray diffraction data were collected at 90.0(2) K on a Bruker D8 Venture dual-source diffractometer with graded-multilayer focused MoK(alpha) X-rays. Raw data were integrated, scaled, merged and corrected for Lorentz-polarization effects using the APEX3 package.[6] Corrections for absorption were applied using SADABS.[7] The structures were solved by dual-space methods (SHELXT[8]) and refined against F^2 by weighted full-matrix least-squares (SHELXL-2018).[9] Hydrogen atoms were found in difference maps but subsequently placed at calculated positions and refined using riding models. Non-hydrogen atoms were refined with anisotropic displacement parameters. The F-ADT core and the ethyl groups were disordered over two sets of positions. The final structure model was checked using established methods.[10,11] Atomic scattering factors were taken from the International Tables for Crystallography.[12] Structures for **TES-FADT** and **TEG-FADT** have been previously reported.[1,2]
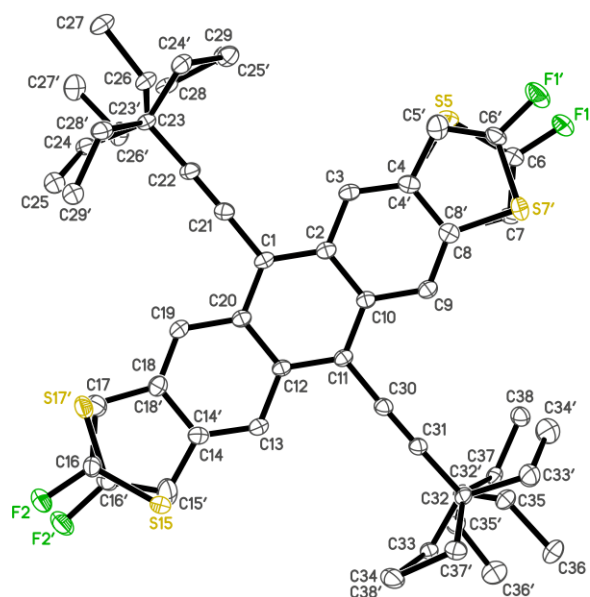
*Figure S 12. Ellipsoid plot (50%) for **TEC-FADT***

Table 1. Crystal data and structure refinement for m20127 (**TEC-FADT**).

Identification code	m20127
Empirical formula	C36 H36 F2 S2
Formula weight	570.77
Temperature	90.0(2) K
Wavelength	0.71073 A
Crystal system, space group	Triclinic, P-1
Unit cell dimensions	a = 10.7452(8) A alpha = 68.595(3) deg.
	b = 11.8352(9) A beta = 79.608(4) deg.
	c = 12.8249(11) A gamma = 77.001(3) deg.
Volume	1470.8(2) A^3
Z, Calculated density	2, 1.289 Mg/m^3
Absorption coefficient	0.218 mm^-1
F(000)	604
Crystal size	0.320 x 0.180 x 0.100 mm

Theta range for data collection	2.070 to 27.499 deg.
Limiting indices	-13<=h<=13, -15<=k<=15, -16<=l<=16
Reflections collected / unique	27694 / 6713 [R(int) = 0.0392]
Completeness to theta = 25.242	99.8 %
Absorption correction	Semi-empirical from equivalents
Max. and min. transmission	0.971 and 0.874
Refinement method	Full-matrix least-squares on F^2
Data / restraints / parameters	6713 / 788 / 546
Goodness-of-fit on F^2	1.084
Final R indices [I>2sigma(I)]	R1 = 0.0458, wR2 = 0.1230
R indices (all data)	R1 = 0.0566, wR2 = 0.1291
Extinction coefficient	0.016(3)
Largest diff. peak and hole	0.356 and -0.231 e.A^-3

Electrochemistry
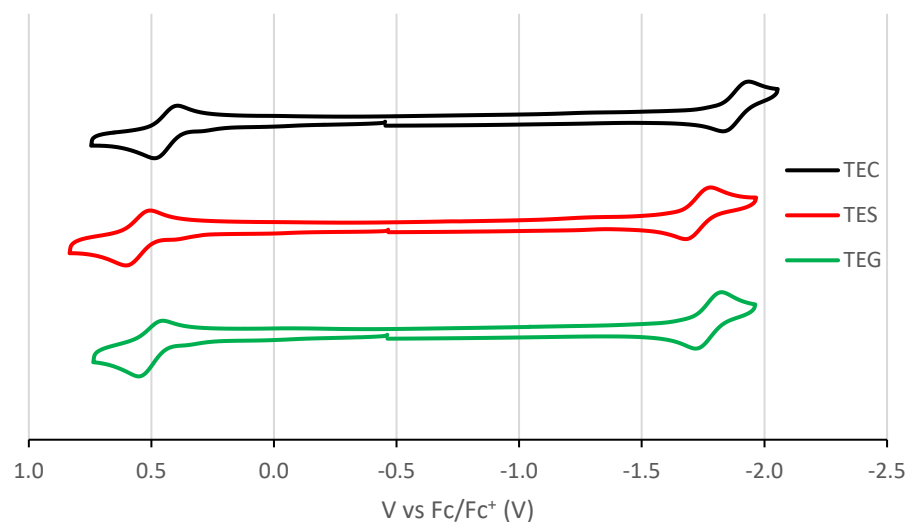
Figure S 13. Cyclic voltammograms of TEC-FADT (black), TES-FADT (red) and TEG-FADT (green) measured in 0.1 M NBu$_4$PF$_6$ in CH$_2$Cl$_2$ at 50 mV/s scan rate versus the oxidation of ferrocene.

Absorption Experiments
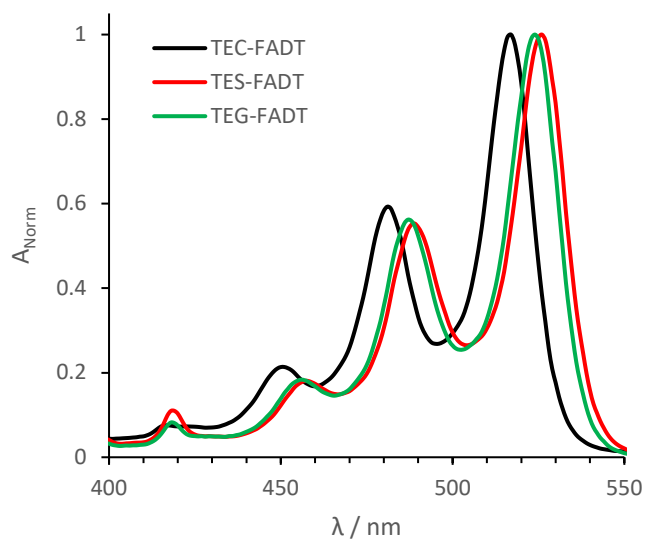
Figure S 14. Comparison of normalized absorption spectra of TEC-FADT (black), TES-FADT (red) and TEG-FADT (green) measured at 298 K in CH_2Cl_2 at 10^{-6} M concentration.
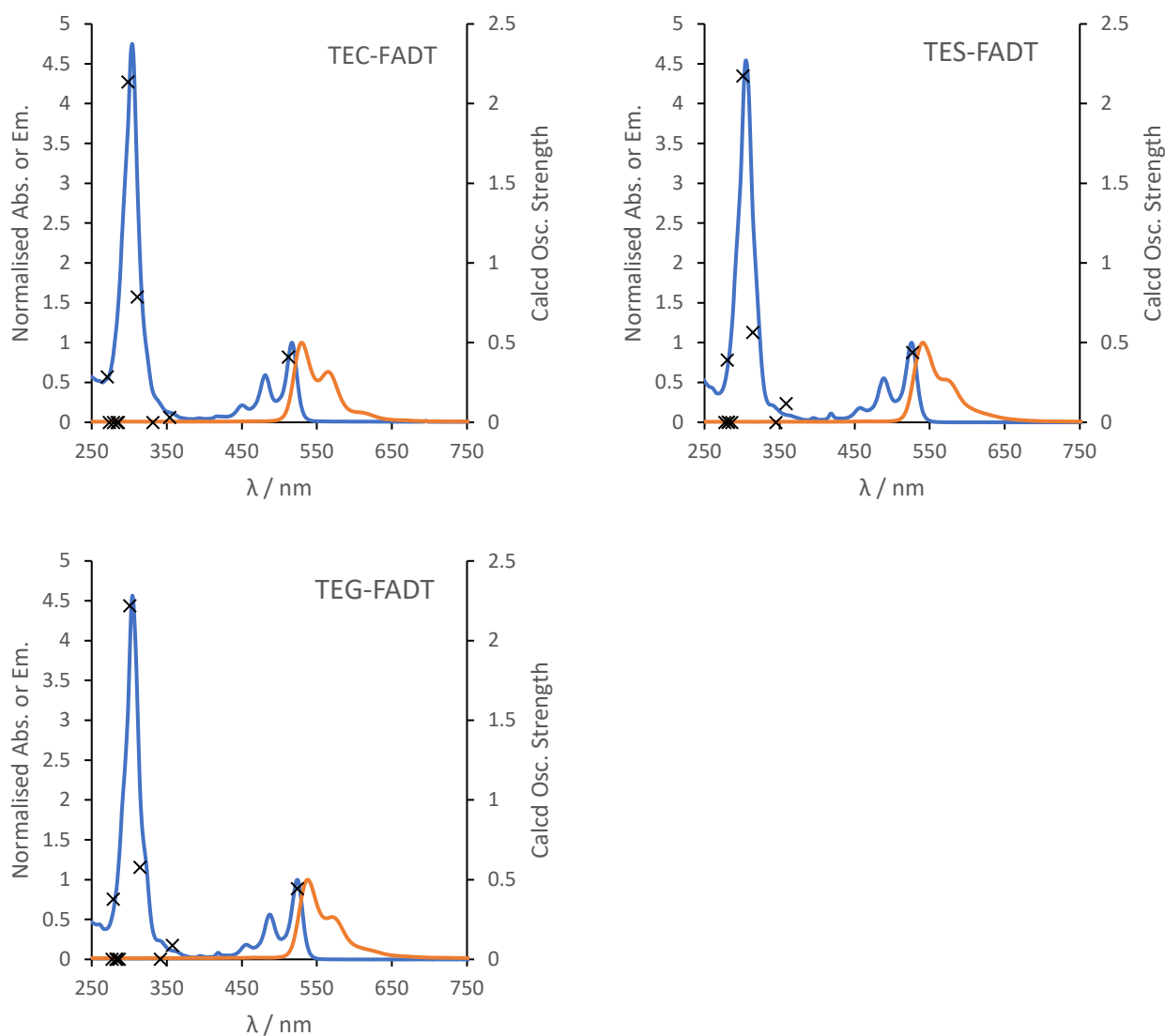
Figure S 15 Experimental absorption (blue), emission (orange) spectra of TEC-FADT (top-left), TES-FADT (top-right) and TEG-FADT (bottom-left) measured at 298 K in CH_2Cl_2 at 10^{-6} M. Crosses indicate the TD-DFT wavelength and oscillator strengths of vertical excitations, calculated with tuned ωB97XD/6-31G* in $CHCl_3$ polarisable continuum.

Photostability experiment details

Photostability measurements were conducted by dissolving the relevant FADT in 2.5 mL of a given solvent, such that the absorbance at λ_{max} in the visible region was around 1 a.u. The sample was then illuminated with a 365 nm LED with estimated luminance of 50,000 Cd/m^2 held 2 inches above the sample cuvette. The absorption spectrum was remeasured every 10 minutes over a 5 hour period. Absorbance (A) at the λ_{max} was normalised against the absorbance at time zero (A_0) and plotted versus time of illumination.

Photostability of NMR samples was conducted by first measuring the ^{1}H spectra of freshly prepared samples, and then keeping the sample tubes in direct sunlight over several days. All samples were prepared within minutes of one another, and then exposed to the exact same light conditions.
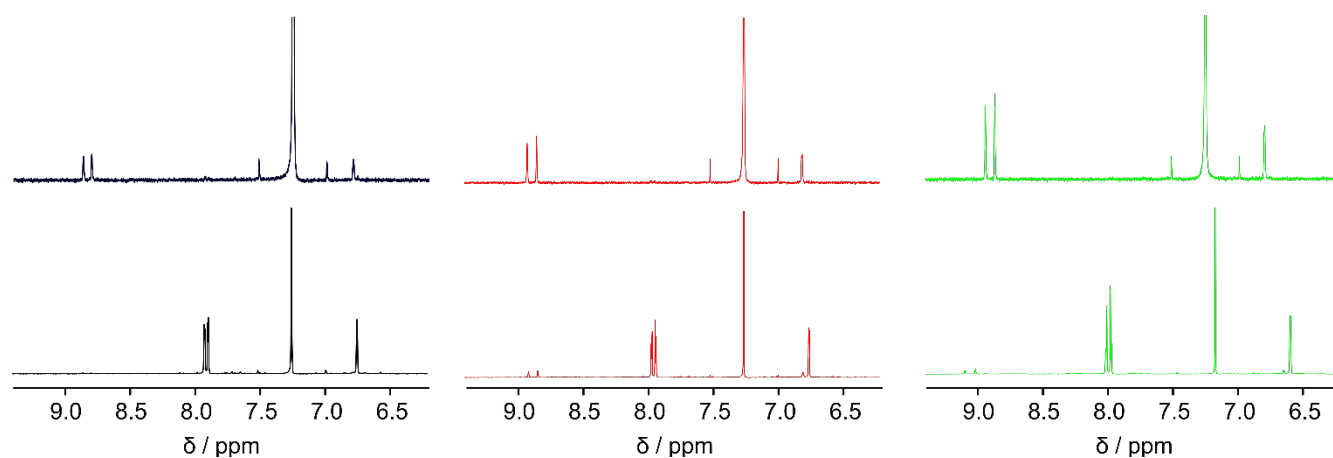
Figure S 16. Aromatic region of ^{1}H NMR of dilute samples of TEC-FADT (black), TES-FADT (red) and TEG-FADT (green) before (top) and after (bottom) light exposure for 1 day. Measured in CDCl$_3$ at 298 K.

Computational Details

Single molecule properties:

Single molecule calculations were run using Gaussian 16 Rev A.02,[13] with natural bond order calculations using the NBO6 software.[14] Calculations for vibrational, redox, and excitation properties were performed with an optimally tuned ωB97XD functional and 6-31G* basis set.[15] All geometries converged with no imaginary frequencies. Franck-Condon analysis was performed by frequency analysis of ground and excited states.[16]
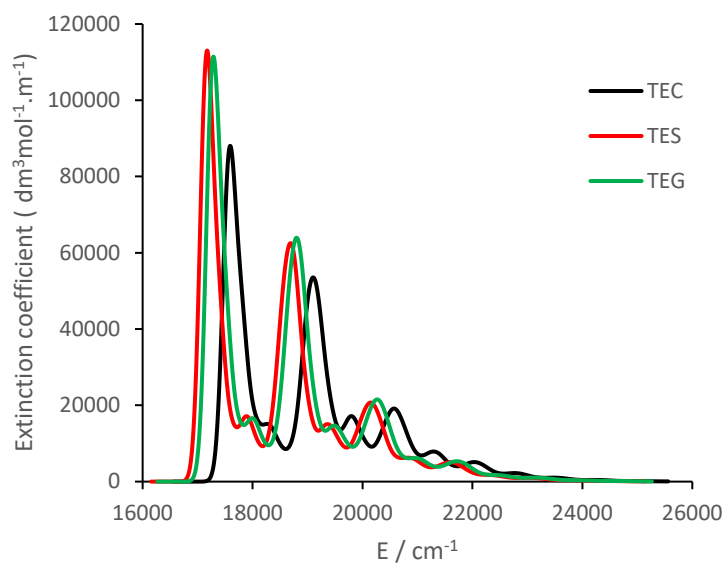
Figure S 17. Simulated absorption spectra for TEC-FADT, TES-FADT and TEG-FADT at 0 K using tuned ωB97XD/6-31G* in chloroform PCM.
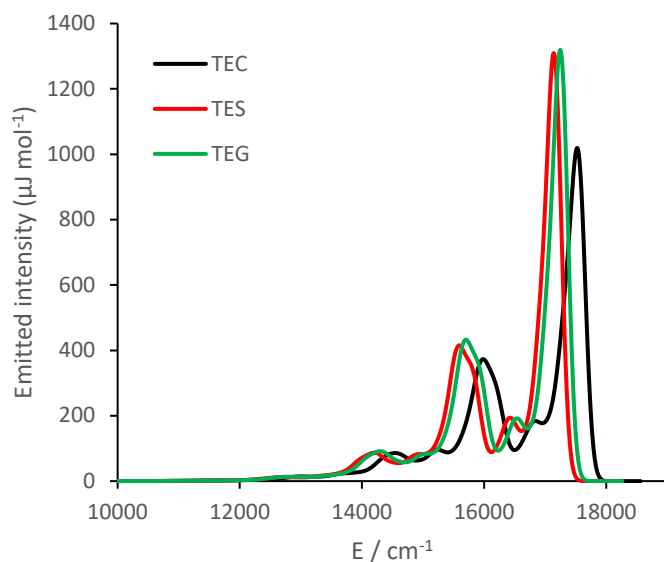
Figure S 18 Simulated emission spectra for TEC-FADT, TES-FADT and TEG-FADT at 0 K using tuned ωB97XD/6-31G* in chloroform PCM.

Natural Bond Orbital (NBO) analysis

NBO analysis was performed using Gaussian 16 Rev A.02 and NBO 6.0. The NBO keyword e2pert=0.1 was used to reduce the cutoff of reported intramolecular perturbation interactions to capture low energy interactions. NBO donor-acceptor interactions involving both alkynyl and C/Si/Ge atom were found from the reported list of interactions, and identified as electron donating (σ-π*) or electron withdrawing (π-σ* and π-d). The stabilization energies of each type of interaction were summed, and reported in Table S5 and Table 2 in the manuscript. All energies are in kcal/mol and represent only one of the alkynyl groups in the case of the FADT series.

Donor NBOs

Alkyne π   Alkyne π   Si-C σ
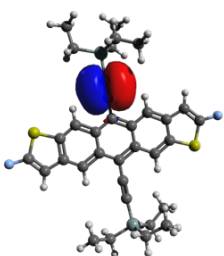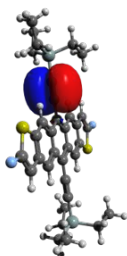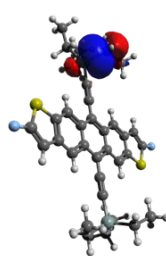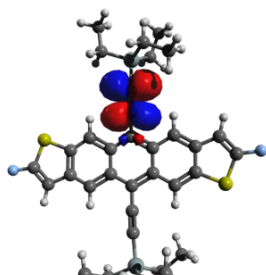
Acceptor NBOs
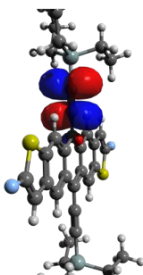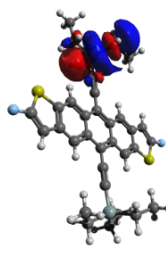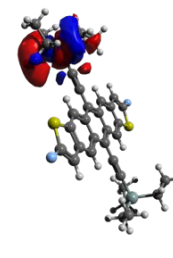
Alkyne π*   Alkyne π*   Si-C σ*   Si Ry (d)

Figure S 19 Examples of donor and acceptor NBOs based on the alkyne and silicon functional groups in the analysis of TES-FADT

Table S 5. NBO perturbation stabilisation energies for electron donating hyperconjugation σ-π*, electron withdrawing hyperconjugation π-σ*, and electron withdrawing π-d interactions in model phenyl molecules. All energies in kcal/mol.

	σ-π*	π-σ*	π-d	Electron Donation
PhCMe₃	5.12	5.6	0.29	-0.77
PhSiMe₃	2.4	5.81	0.93	-4.34
PhGeMe₃	2.77	5.71	0	-2.94

Calculations to determine photoreaction enthalpies were run in Gaussian 16. All calculations, geometry and frequency, were run with an M06-2X functional and cc-pvdz basis set corrected with a D3 dispersion. All geometries converged with no imaginary frequencies. The calculated sums of electronic and thermal enthalpies from the output files were used to determine overall changes in the enthalpies of the proposed light induced reaction of FADT derivatives.

Table S 6. Computed reaction enthalpies for potential photoreactions of FADTs

Change in Enthalpy (KJ/mol)	TEC-FADT	TES-FADT	TEG-FADT
Dimerization	18.53	14.83	14.63
Oxidation	-10.32	-3.65	-4.89
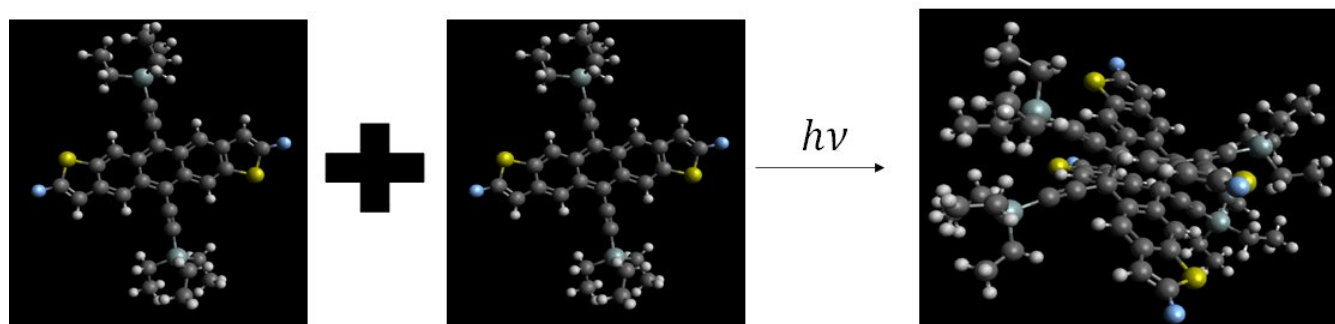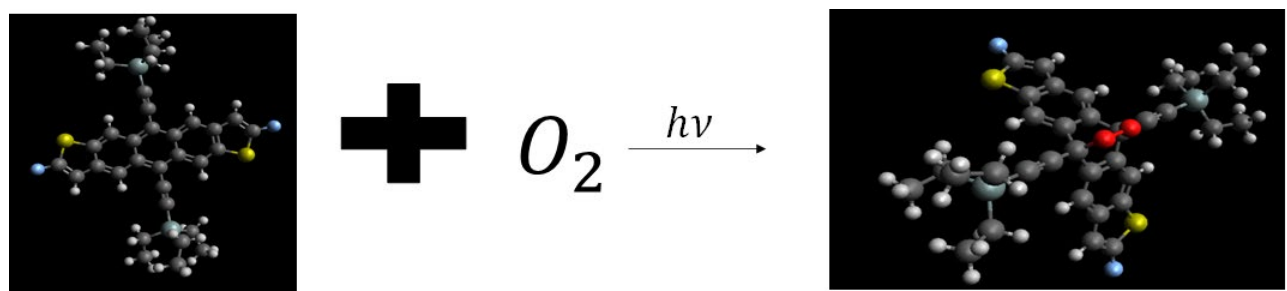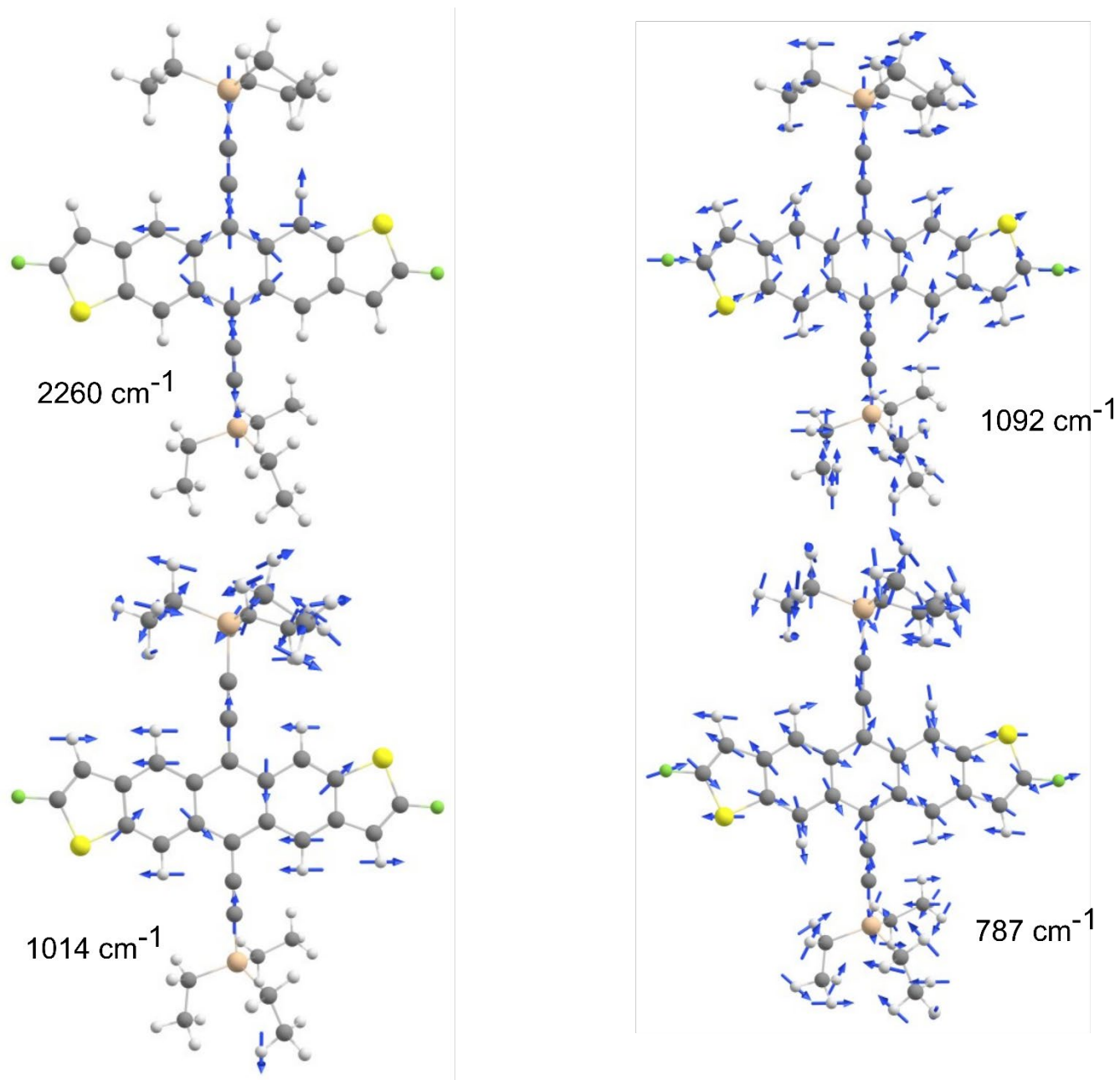
Figure S 20. Selected vibrational modes in TES-FADT, corresponding to the peaks which are observed to be more intense in FTIR spectra of TES-FADT than TEC-FADT.
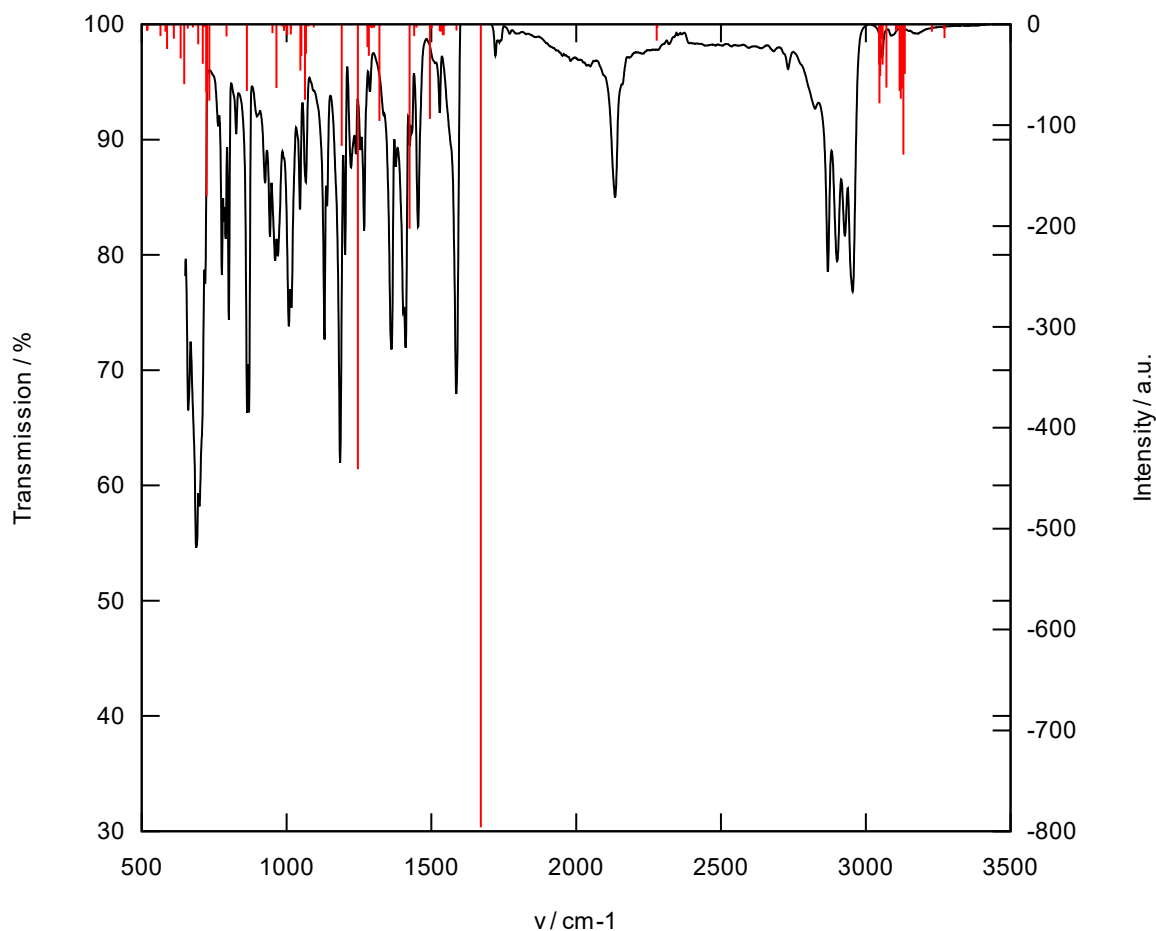
Figure S 21. Experimental FTIR spectrum of TEG-FADT (black) and computed IR spectrum (red) using tuned ωB97XD/6-31G*

Side chain interactions:

Side group interactions were performed using the MOPAC software[17] and the PM7 semi-empirical method which contains dispersion interactions for proper intermolecular description. Calculations were performed between molecules of fixed distance and orientation, with the alkyl chains allowed to relax as per our previous study.[18] Three calculations with different starting points were calculated per data point, with the lowest resulting energy used for analysis.
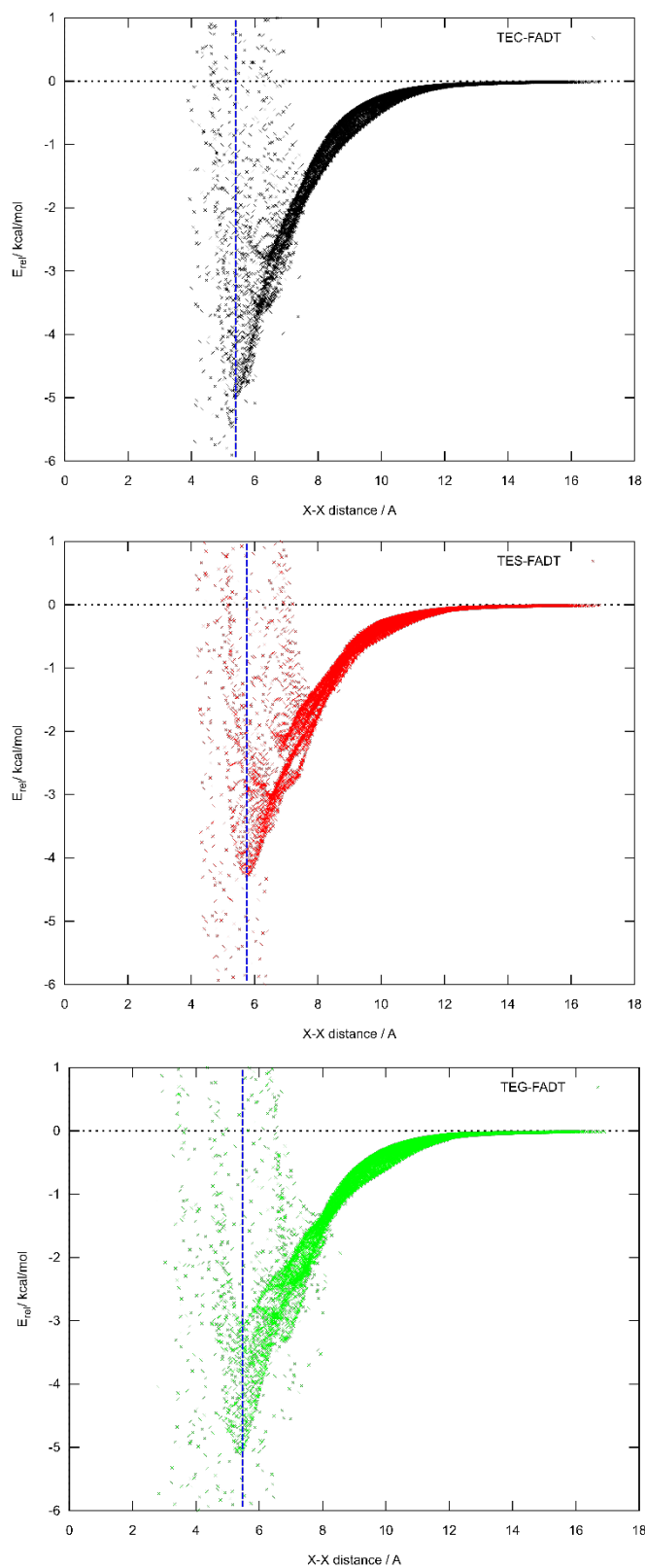
Figure S 22. PM7 calculated interaction energies between side chains as a function of C-C, Si-Si. Or Ge-Ge distance. Blue lines provide an estimate of the radius of the side chains.

Hypothetical unit cell optimization:

Unit cell optimisations were performed using Quantum Espresso[19,20] using PBE0 functional with DFT-D3 dispersion correction and projector-augmented wave (PAW)[21] method, with pseudopotentials from pslibrary[22] and a kinetic energy cutoff of 80 Ry. Unit cell optimization used a Monkhorst−Pack grid of 4×3×3 for 2D packing and 2×2×2 for 1D packing. Binding energies were calculated by first increasing the unit cell size until the energy of unit cell constrained optimisations converged, thus representing the gas phase molecular energy. These calculations were performed at only the Γ-point. Binding energy per molecule was then found by:

$$E_{binding} = \frac{E_{UC}}{N_{UC}} - E_{mol}$$

where E_{UC} is the energy of the optimized unit cell, N_{UC} is the number of molecules per unit cell, and E_{mol} is the energy of an isolated molecule. Only major occupancies of disordered atoms were considered.

Table S 7 Binding energies per molecule for TEC-, TES-, and TEG-FADT in optimised unit cells starting from TEC-,TES- or TEG-FADT crystal structures. All energies in kJ/mol

	TEC Packing	TES Packing	TEG Packing
TEC-FADT	-343.2	-323.0	-319.8
TES-FADT	-332.0	-337.2	-338.5
TEG-FADT	-331.1	-337.2	-342.9

Symmetry adapted perturbation theory (SAPT0)[23] calculations on close pairs of molecules were performed using Psi4 software[24] using the jun-cc-pvdz basis set.
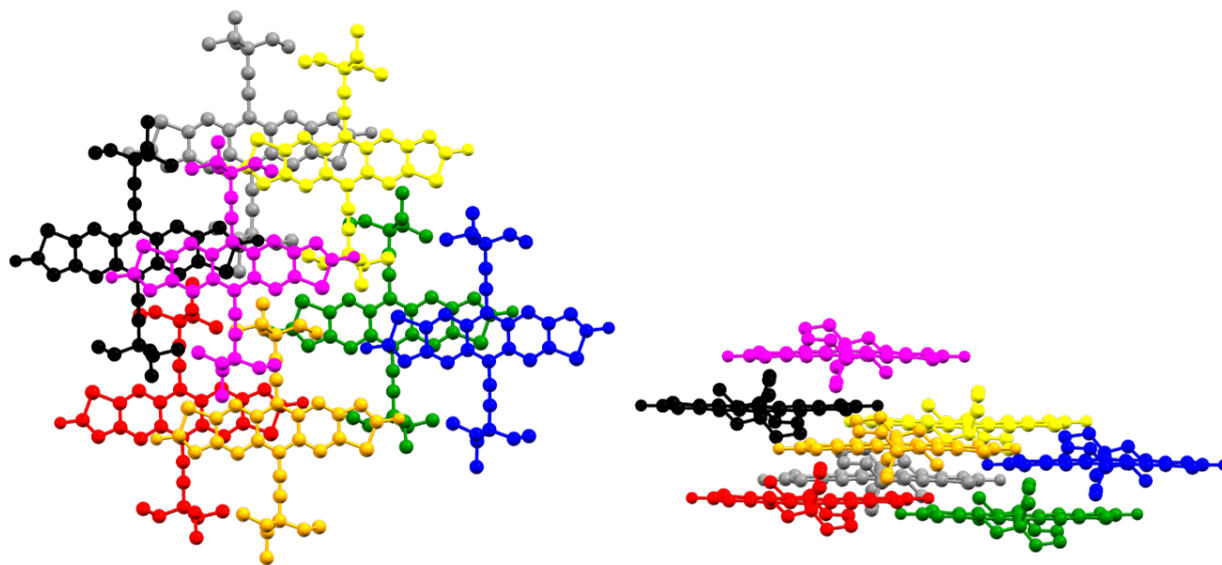
Contact	TEC-FADT 1D	TES-FADT 1D	Difference
Orange-to-Blue	**-2.93**	**-2.31**	**-0.62**
Orange-to-Black	-4.85	-4.72	-0.13
Orange-to-Green	**-6.49**	**-5.64**	**-0.85**
Orange-to-Pink	-8.91	-9.26	0.35
Orange-to-Grey	-1.25	-1.15	-0.10
Orange-to-Yellow	-2.43	-2.50	0.07
Orange-to-Red	-28.15	-28.05	-0.11

Table S 8. Pairwise total SAPT0/jun-cc-pvdz energies for TEC-FADT in its native 1D packing, and TES-FADT in a hypothetical 1D packing. Values in bold (in-plane H…F interaction, and sidechain-to-pi interaction) are deemed the most influential in TEC-FADT preferring the 1D packing rather than TES-FADT.
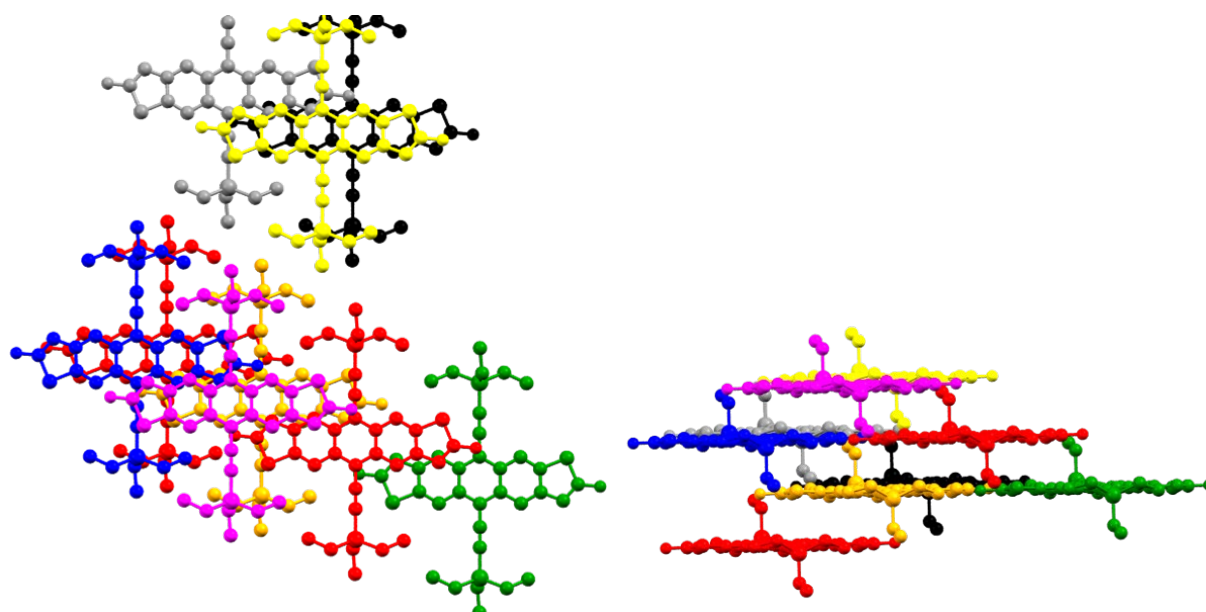
Contact	TES-FADT 2D	TEC-FADT 2D	Difference
Orange-to-Green	-3.18	-3.14	-0.04
Orange-to-Black	-1.89	-1.52	-0.37
Orange-to-Grey	-1.63	-1.66	0.03
Orange-to-Yellow	-1.91	-1.93	0.02
Orange-to-Pink	**-4.53**	**-3.48**	**-1.05**
Orange-to-Red	**-25.91**	**-25.15**	**-0.76**
Orange-to-Blue	**-18.76**	**-17.77**	**-0.99**

Table S 9. Pairwise total SAPT0/jun-cc-pvdz energies for TES-FADT in its native 2D packing, and TEC-FADT in a hypothetical 2D packing. Values in bold are discussed further in the main text.
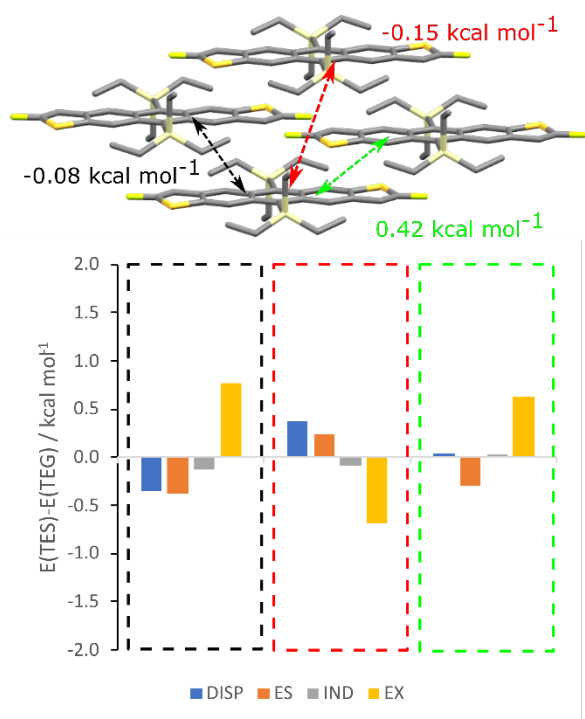
Figure S 23. Difference in SAPT energies between TES-FADT and TEG-FADT in optimized 2D packing.

References

1   S. Subramanian, K. P. Sung, S. R. Parkin, V. Podzorov, T. N. Jackson and J. E. Anthony, *J. Am. Chem. Soc.*, 2008, **130**, 2706–2707.

2   Y. Mei, M. A. Loth, M. Payne, W. Zhang, J. Smith, C. S. Day, S. R. Parkin, M. Heeney, I. McCulloch, T. D. Anthopoulos, J. E. Anthony and O. D. Jurchescu, *Adv. Mater.*, 2013, **25**, 4352–4357.

3   S. Arseniyadis, K. S. Kyler and D. S. Watt, in *Organic Reactions*, Wiley, 1984, pp. 1–364.

4   F. C. Whitmore and C. E. Lewis, *J. Am. Chem. Soc.*, 1942, **64**, 1618–1619.

5   W. Priester and R. West, *J. Am. Chem. Soc.*, 1976, **98**, 8421–8425.

6   Bruker-AXS, 2018.

7   L. Krause, R. Herbst-Irmer, G. M. Sheldrick and D. Stalke, *J. Appl. Crystallogr.*, 2015, **48**, 3–10.

8   G. M. Sheldrick, *Acta Crystallogr. Sect. A Found. Crystallogr.*, 2015, **71**, 3–8.

9   G. M. Sheldrick, *Acta Crystallogr. Sect. C Struct. Chem.*, 2015, **71**, 3–8.

10 S. Parkin, *Acta Crystallogr. Sect. A Found. Crystallogr.*, 2000, **56**, 157–162.

11 A. L. Spek, *Acta Crystallogr. Sect. D Biol. Crystallogr.*, 2009, **65**, 148–155.

12 A.J.C. Wilson, *International Tables for Crystallography, vol C: Mathematical, Physical and Chemical Tables*, Kluwer Academic Publishers, Holland, 1992.

13 M. J. Frisch, G. W. Trucks, H. B. Schlegel, G. E. Scuseria, M. A. Robb, J. R. Cheeseman, G. Scalmani, V. Barone, G. A. Petersson, H. Nakatsuji, X. Li, M. Caricato, A. V. Marenich, J. Bloino, B. G. Janesko, R. Gomperts, B. Mennucci, H. P. Hratchian, J. V. Ortiz, A. F. Izmaylov, J. L. Sonnenberg, D. Williams-Young, F. Ding, F. Lipparini, F. Egidi, J. Goings, B. Peng, A. Petrone, T. Henderson, D. Ranasinghe, V. G. Zakrzewski, J. Gao, N. Rega, G. Zheng, W. Liang, M. Hada, M. Ehara, K. Toyota, R. Fukuda, J. Hasegawa, M. Ishida, T. Nakajima, Y. Honda, O. Kitao, H. Nakai, T. Vreven, K. Throssell, J. J. A. Montgomery, J. E. Peralta, F. Ogliaro, M. J. Bearpark, J. J. Heyd, E. N. Brothers, K. N. Kudin, V. N. Staroverov, T. A. Keith, R. Kobayashi, J. Normand, K. Raghavachari, A. P. Rendell, J. C. Burant, S. S. Iyengar, J. Tomasi, M. Cossi, J. M. Millam, M.

Klene, C. Adamo, R. Cammi, J. W. Ochterski, R. L. Martin, K. Morokuma, O. Farkas, J. B. Foresman and D. J. Fox, *Gaussian 16, Revision A.02*, Gaussian, Inc., Wallingford CT, 2016.

14   E. D. Glendening, J. K. Badenhoop, A. E. Reed, J. E. Carpenter, J. A. Bohmann, C. M. Morales, C. R. Landis and F. Weinhold, *NBO 6.0*, Theoretical Chemistry Institute, University of Wisconsin, Madison, 2013.

15   M. Moser, K. J. Thorley, F. Moruzzi, J. F. Ponder, I. P. Maria, A. Giovannitti, S. Inal and I. McCulloch, *J. Mater. Chem. C*, 2019, **7**, 5359–5365.

16   V. Barone, J. Bloino, M. Biczysko and F. Santoro, *J. Chem. Theory Comput.*, 2009, **5**, 540–554.

17   H. A. Kurtz, J. J. P. Stewart and K. M. Dieter, *J. Comput. Chem.*, 1990, **11**, 82–87.

18   K. J. Thorley, T. W. Finn, K. Jarolimek, J. E. Anthony and C. Risko, *Chem. Mater.*, 2017, **29**, 2502–2512.

19   P. Giannozzi, S. Baroni, N. Bonini, M. Calandra, R. Car, C. Cavazzoni, D. Ceresoli, G. L. Chiarotti, M. Cococcioni, I. Dabo, A. Dal Corso, S. De Gironcoli, S. Fabris, G. Fratesi, R. Gebauer, U. Gerstmann, C. Gougoussis, A. Kokalj, M. Lazzeri, L. Martin-Samos, N. Marzari, F. Mauri, R. Mazzarello, S. Paolini, A. Pasquarello, L. Paulatto, C. Sbraccia, S. Scandolo, G. Sclauzero, A. P. Seitsonen, A. Smogunov, P. Umari and R. M. Wentzcovitch, *J. Phys. Condens. Matter*, 2009, **21**, 395502.

20   P. Giannozzi, O. Andreussi, T. Brumme, O. Bunau, M. Buongiorno Nardelli, M. Calandra, R. Car, C. Cavazzoni, D. Ceresoli, M. Cococcioni, N. Colonna, I. Carnimeo, A. Dal Corso, S. De Gironcoli, P. Delugas, R. A. Distasio, A. Ferretti, A. Floris, G. Fratesi, G. Fugallo, R. Gebauer, U. Gerstmann, F. Giustino, T. Gorni, J. Jia, M. Kawamura, H. Y. Ko, A. Kokalj, E. Kücükbenli, M. Lazzeri, M. Marsili, N. Marzari, F. Mauri, N. L. Nguyen, H. V. Nguyen, A. Otero-De-La-Roza, L. Paulatto, S. Poncé, D. Rocca, R. Sabatini, B. Santra, M. Schlipf, A. P. Seitsonen, A. Smogunov, I. Timrov, T. Thonhauser, P. Umari, N. Vast, X. Wu and S. Baroni, *J. Phys. Condens. Matter*, 2017, **29**, 465901.

21   P. E. Blöchl, *Phys. Rev. B*, 1994, **50**, 17953–17979.

22   A. Dal Corso, *Comput. Mater. Sci.*, 2014, **95**, 337–350.

23   E. G. Hohenstein and C. D. Sherrill, *J. Chem. Phys.*, 2010, **132**, 184111.

24   J. M. Turney, A. C. Simmonett, R. M. Parrish, E. G. Hohenstein, F. A. Evangelista, J. T. Fermann, B. J. Mintz, L. A. Burns, J. J. Wilke, M. L. Abrams, N. J. Russ, M. L. Leininger, C. L. Janssen, E. T. Seidl, W. D. Allen, H. F. Schaefer, R. A. King, E. F. Valeev, C. D. Sherrill and T. D. Crawford, *Wiley Interdiscip. Rev. Comput. Mol. Sci.*, 2012, **2**, 556–565.